Medical Hypotheses 131 (2019) 109305

Contents lists available at ScienceDirect

Medical Hypotheses

journal homepage: www.elsevier.com/locate/mehy

Possible role of rivoglitazone thiazolidine class of drug as dual-target therapeutic agent for bacterial infections: An *in silico* study

Vidyasrilekha Yele*, Niladri Saha, Afzal Azam Md

Department of Pharmaceutical Chemistry, JSS College of Pharmacy, Ootacamund, JSS Academy of Higher Education & Research, Mysuru 643001, India

ARTICLE INFO

Keywords:
Rivoglitazone
ParE
MurE
Docking
MM-GBSA
Molecular dynamic simulations
Anti-bacterial agent

ABSTRACT

Infections due to resistant bacteria are the life-threatening and leading cause of mortality worldwide. The current therapy for bacterial infections includes treatment with various drugs and antibiotics. The misuse and over usage of these antibiotics leads to bacterial resistance. There are several mechanisms by which bacteria exhibit resistance to some antibiotics. These include drug inactivation or modification, elimination of antibiotics through efflux pumps, drug target alteration, and modification of metabolic pathway. However, it is difficult to treat infections caused by resistant bacteria by conventional existing therapy. In the present study binding affinities of some glitazones against ParE and MurE bacterial enzymes are investigated by *in silico* methods. As evident by extra-precision docking and binding free energy calculation (MM-GBSA) results, rivoglitazone exhibited higher binding affinity against both ParE and MurE enzymes compared to all other selected compounds. Further molecular dynamic (MD) simulations were performed to validate the stability of rivoglitazone/4MOT and rivoglitazone/4C13 complexes and to get insight into the binding mode of inhibitor. Thus, we hypothesize that structural modifications of the rivoglitazone scaffold can be useful for the development of an effective antibacterial agent.

Introduction

Bacterial infections are life-threatening and increased the mortality rate of infected people. However, there is a significant decrease in the death rate of the patients over the past decade, by 'wonder drugs' called antibiotics [1]. The misuse and over usage of these antibiotics lead to antimicrobial resistance (AMR), a global threat. The major multidrug resistance (MDR) and extensive drug resistance (XDR) exhibiting by the ESKAPEpathogens. These include six nosocomial pathogens i.e. E. faecium, S. aureus, K. pneumoniae, A. baumannii, P. aeruginosa, and Enterobacter species throughout the world [2]. Though, there are several marketed formulations available, against the nosocomial infection [3]. But all these pathogens exhibit resistance against antibiotics through various mechanisms such as drug inactivation or target (penicillinases, cephalosporinases, carbapenemases, β-lactamases play role in inactivation of penicillin, cephalosporins and carbapenems respectively) [4], modification of binding sites (penicillin-binding proteins, PBP2a in *S. aureus*, changing the cross-linking target of peptidoglycan layer in *E. faecium* and *E. faecalis* develop resistance against vancomycin and teicoplanin) [5], porin loss (the reduced level of OprD porin protein in *P. aeruginosa* exhibits resistance against imipenem) [6], efflux pumps (polyselective efflux pump, RND superfamily plays a key role in MDR bacterial phenotype) [7]. In the last decade, the antibiotic linezolid (2000) exhibited resistance against *Staphylococcus* in 2001, daptomycin (2003) availed resistance against *Acinetobacter* and *Pseudomonas* in 2004 and 2005 respectively, ceftaroline (2010) developed resistance against *Neisseria*, *Staphylococcus*, *Enterobacteriaceae* in 2011 [8–10]. As per the statistics by Jim O'Neill [11], 70,000 infected people in the world were prone to death as of 2017 and estimated that there will be an increase to 10 million people each year by 2050. Hence urgent attention is required to combat the consistent rise of bacterial resistance.

Many targets have been studied for the development of antibacterial agents [1]. Cell wall biosynthesis pathway has been extensively studied and validated as antibacterial targets by β-lactam and glycopeptide classes of antibiotics. Though, these antibiotics proven to be clinically significant, it warrants the development of novel antibacterial agents due to the emergence of resistance [12]. The cell wall of bacteria is made up of peptidoglycan layer, a few antibacterial agents inhibit the biosynthesis and polymerization of peptidoglycan by targeting Mur ligases namely MurA, MurB, MurC, MurD, MurE, MurF [13]. 2. Fatty acid biosynthesis pathway has also been validated by the extensive use of known drugs like Isoniazid, anti-tubercular drug and triclosan, antiseptic [14]. 3. RNA polymerase, multi sub-unit complex is a key functional enzyme necessary for the bacterial growth [15]. The DNA

* Corresponding author.
E-mail addresses: vslphd@jssuni.edu.in (V. Yele), afzal@jssuni.edu.in (A.A. Md).

https://doi.org/10.1016/j.mehy.2019.109305
Received 1 May 2019; Received in revised form 18 June 2019; Accepted 5 July 2019

dependent RNA polymerase (RNAP) is an attractive target in bacteriology, the inactivation of which leads to bacterial cell death [4]. This pathway has been validated by some of the antibiotics like rifamycin, antitubercular drug and it is a potent inhibitor of *E. coli* RNAP with a *Ki* value of ~1 nM. 4. Bacterial folate biosynthesis is a known attractive target and includes two types of enzyme, DHFR (dihydrofolate reductase) and DHPS (dihydropteroate synthase). The first and foremost enzyme DHFR has been validated by the known antibacterial drug, trimethoprim and also an anti-protozoal drug, pyrimethamine. The second enzyme DHPS has been proved as an essential target after its validation by sulphonamide, acting along with the DHFR synergistically [16]. The use of anti-folates results in the thymine less death of the bacterial cell [17]. 5. Dual inhibition of DNA GyrB and ParE is also one of the effective antibacterial targets. The inhibition of these topoisomerases results in the prevention of DNA replication, repair and DNA catenation [18]. 6. Protein synthesis mainly carried out by the molecular machinery called ribosomes and the translational machinery considered as a major target for the antibacterial drugs [19]. Many antibacterial drugs targeting the protein synthesis are tetracyclines (blocks the A site of 30S subunit of ribosome thereby preventing the binding of aminoacyl t-RNA) [20], aminoglycosides (interferes with the formation of initiation complexes of 30S subunit) [21], macrolides (interferes with elongation of peptide during transpeptidation cycle) [22].

The two major challenges encountered in the development of novel antibacterial agents include proper selection of specific target, particularly molecular targets which are not prone to AMR rapidly. The second challenge involves improvement of libraries of chemical compounds to overcome the disadvantages associated with diversity, barriers to permeation of the drug through cell wall [23]. So, to combat these problems the new approaches have been put-forth, application of existing drugs of other classes and multi-targeting phenomenon. Thiazolidine ring has been reported to confer antibacterial activity against various targets. The drug pioglitazone, an antidiabetic drug which contains thiazolidine moiety acts as an antibacterial drug in a dose-dependent manner with an optimal concentration of 80 μg/ml [24]. The chemical structures 1–3 possessing thiazolidine moiety are investigated by Opperman et al., [25] (Fig. 1). Authors revealed that the rhodanines bearing thiazolidine moiety exhibit antibacterial activity specifically by inhibiting the initial developmental stages of bio-film, thereby preventing the adhesion of bacterial cell membrane to the surface. Derivatives of rhodanines are investigated by Tomasic et al. [25] for their antibacterial activity. These compounds exhibited promising activity against methicillin-resistant *S. aureus* (MRSA). The compounds have significantly higher potency when compared to standard antibiotic like norfloxacin. The compound 4 (Fig. 1) exhibited significant inhibition with minimum inhibitory concentration (MIC) of 0.5 and 32 μg/ml against *S. aureus* and MRSA, respectively [25]. Rivoglitazone a peroxisome proliferating activating receptor (PPAR-γ) agonist is reported to possess minor dose-dependent adverse effects like peripheral edema and weight gain [26]. Moreover, the thiazolidine-2,4-dione moiety inhibiting the bacteria by targeting various mechanisms, it is hereby hypothesized that the rivoglitazone, thiazolidine-2,4-dione, class of drug may act as a potential antibacterial agent. In the present study, we used combined molecular modeling approaches to show that rivoglitazone have high binding affinity against both ParE and MurE bacterial enzymes. ParE belongs to the class of topoisomerases which involves in the decatenation of daughter chromatids behind the replication fork [27]. MurE has a prominent role in peptidoglycan synthesis of the bacterial cell wall [28] which has been validated using computational tools like docking, binding free energy calculations molecular dynamic (MD) simulations.

Methodology

Protein preparation

Computational studies were performed using the Schrödinger suite 2018-1 (LLC, NY, USA). Two different targets proteins ParE (pdb.4MOT, resolution 1.75 Å) and MurE (pdb.4C13, resolution 1.9 Å) were selected for the current study. The three-dimensional structures of these enzymes were downloaded from RCSB-protein data bank (RCSB-PDB) (www.rcsb.org/pdb) in *.pdb* format. The receptor crystal structures were chosen based on the different parameters like resolution, completeness, expression system, source organism, cocrystal ligand, etc. The details of the receptor structures were provided in Table 1. The X-ray crystal structure of the receptor was prepared using the protein preparation wizard, Schrödinger suite 2018-1 [29]. The water molecules were removed, hydrogen bonds (pH 7+/−2) and missing side chain atoms were added before protein optimization [30]. The receptor grid was generated within a radius 10 Å which defines the centroid of the active site of bound ligand. The stereological aspect of the enzyme's backbone, Ramachandran plots were generated under the protein preparation wizard of Schrödinger suite 2018-1 module.

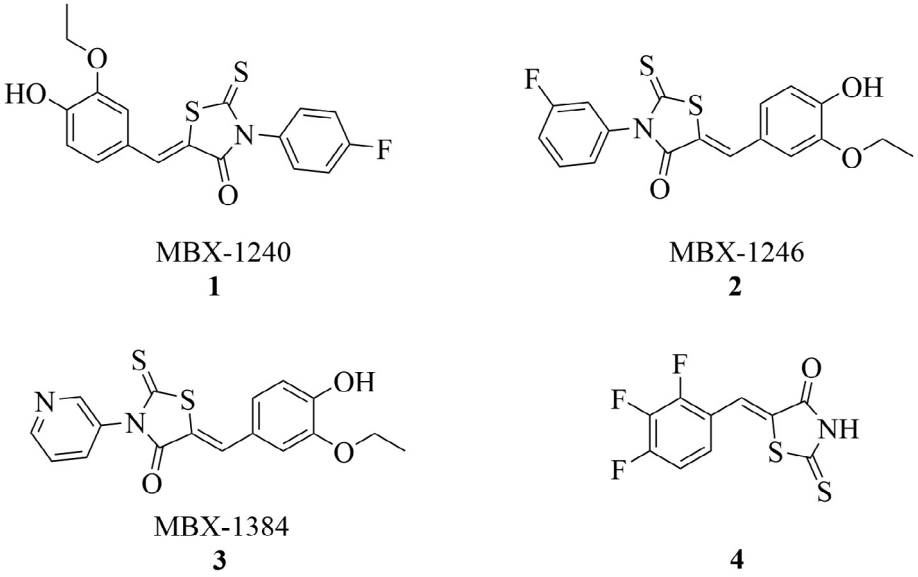

Fig. 1. Chemical structures of 4 molecules containing the thiazolidine ring.

Table 1
Details of the receptors and its bound ligand used in the current study. Stereological aspect of the receptors was studied using Schrödinger 2018-1 suite, and the % residues of the receptors in the allowed and disallowed regions of the Ramachandran plot are shown.

Name of the Receptor (PDB ID)	No. of residues	Co-crystal ligand	Resolution; R-factor; R-free	% of residues in different regions		References
				Allowed region	Disallowed region	
ParE (4MOT)	226	AZ13072886	1.75; 0.190; 0.228	95.5%	4.42%	Kale et al. [45]
MurE (4C13)	501	UDP-MurNAc-Ala-Glu-Lys	1.9; 0.196; 0.241	98%	2.7%	Ruane et al. [46]

Table 2
Details of the Ligands used in the current study. HBD: Hydrogen bond donor groups; HBA: Hydrogen bond acceptor groups.

Name of the ligand	PubChem compound ID	Mol. Wt. (g/mol)	Mol. Formula	No. of HBD	No. of HBA	Type of ligand
Novobiocin	54675769	612.632	$C_{13}H_{36}N_2O_{11}$	4	11	Antibacterial
Ciglitazone	2750	333.446	$C_{18}H_{23}NO_3S$	1	4	Antidiabetic
Pioglitazone	4829	356.446	$C_{19}H_{20}N_2O_3S$	1	5	Antidiabetic
Darglitazone	60870	420.483	$C_{23}H_{20}N_2O_4S$	1	6	Antidiabetic
Englitazone	60303	353.436	$C_{20}H_{19}NO_3S$	1	4	Antidiabetic
Rosiglitazone	77999	357.428	$C_{18}H_{19}N_3O_3S$	1	6	Antidiabetic
Netoglitazone	204109	381.421	$C_{12}H_{16}FNO_3S$	1	5	Antidiabetic
Rivoglitazone	3055168	397.449	$C_{20}H_{19}N_3O_4S$	1	6	Antidiabetic

Ligand preparation

The ligands containing thiazolidine moieties such as pioglitazone, darglitazone, englitazone, ciglitazone, rosiglitazone, netoglitazone, and rivoglitazone were selected for the current hypothetical study. The three-dimensional structures of the ligands were selected from the database of NCBI PubChem compounds in *.sdf* format and generated using the builder panel in Maestro 10.2 and optimization was performed for the ligands using LigPrep module [31]. (v3.4, Schrödinger 2018-1). The details of the ligands were provided in Table 2. The standard novobiocin was extracted from the PubChem database in *.sdf* format and was likewise optimized using the module LigPrep. The low-energy conformers of each ligand were obtained after optimization using OPLS3 force field [31].

Molecular docking and binding free energy calculation (MM-GBSA)

To determine the target proteins-ligands binding affinities and optimal geometry of ligands within the active sites, extra-precision docking was performed using Schrödinger suite 2018-1. Binding free energies of selected ligands/4MOT and ligands/4C13 complexes were calculated using the MM-GBSA approach by Prime (v4.0, Schrödinger 2018-1). The minimization of docked poses of ligands in the active pockets of ParE and MurE were performed using the local optimization wizard available in Prime module. The energy calculations of the receptor-ligand complexes were performed using OPLS3 force field and continuum solvent (VSGB 2.0) model [32].

Molecular dynamics (MD) simulations

The MD simulations [33] were performed for the investigative drug rivoglitazone with ParE enzyme (pdb.4MOT) and (pdb.4C13) using the OPLS3 force field [31]. Solvation was achieved for both the systems in orthorhombic boxes utilizing TIP4P water within the Desmond MD system (v4.2) [34,35]. The neutralization of the systems was done by counter ions addition. Limited memory Broyden-Fletcher-Goldfarb-Shanno (LBFGS) minimization of each system was performed with 10 steepest descent steps and 3 vectors to a gradient threshold of 25 kcal/mol/Å. During minimization, maximum iterations were 2000 and the convergence threshold was kept at 1.0 kcal/mol/Å. The long-range interactions (tolerance of 1e − 09) and cut-off radius (9 Å) was applied for short-range coulomb and van der Waals interactions by using the smooth particle mesh Ewald method [36]. 10 ns MD simulations were performed for each system under NPT conditions with the pressure of 1 bar and a temperature of 300 °K [37]. These NPT conditions were maintained by selecting the versatile methods of Martyna-Tobias-Klein and Nose-Hoover thermostat [38,39].

Results

Stereological quality of the receptors

The stereological aspects of the prepared proteins were assessed by generating the Ramachandran plots of the ParE and MurE which were found to exhibiting 95.5 and 98% of the residues in the allowed regions respectively (Table 1). This satisfies the pre-requisite quality of the receptors for computational studies.

Docking poses of the ligands with receptors

When the ligand binds to the receptor with high affinity (i.e., more negative glide score and negative free energy) compared to the standard inhibitor, novobiocin, implicit better inhibitory activity of the target proteins. The docking results of the ligands were provided in Tables 4 and 5. The results of docking studies revealed that the ligands containing thiazolidine moiety bind to the catalytic pocket of the respective receptors, ParE and MurE (Figs. 2 and 3). Further, selected ligands showed interactions at the same site of binding pocket compared to the novobiocin. The docking results and free energy calculations of novobiocin were shown in Table 3.

Inhibition of the receptor activity

The ligand when docked with receptors, the glide score obtained computationally infers about the inhibitory activity of the ligand to the particular receptor. In general, rivoglitazone, showed higher glide score against both target proteins ParE (−5.24 kcal/mol, Table 4) and MurE (−4.88 kcal/mol, Table 5) compared to the other glitazones.

Table 3
Table showing Docking results and binding free energy calculation results of novobiocin (kcal/mol).

Ligand	Receptor (PDB ID)	Docking score	MM-GBSA
Novobiocin	ParE (4MOT)	−5.174	−51.912
	MurE (4C13)	−7.985	−88.52

Table 4
Table showing docking results of selected ligands in the catalytic pocket of ParE enzyme (pdb.4MOT).

Ligands	[a]G_{score}	[b]G_{vdw}	[c]G_{coul}	[d]G_{energy}	[e]G_{model}	[f]H_{Bond}
Ciglitazone	−3.26	−26.042	−3.966	−30.008	−40.365	−0.35
Pioglitazone	−4.239	−34.825	−6.374	−41.199	−55.521	−0.867
Englitazone	−5.563	−37.398	−4.307	−41.705	−51.276	−0.973
Darglitazone	−4.497	−44.049	−2.741	−46.79	−62.156	−0.897
Rosiglitazone	−4.42	−40.017	−6.18	−46.197	−54.675	−0.998
Netoglitazone	−4.751	−36.273	−1.631	−37.905	−49.394	−0.412
Rivoglitazone	−5.204	−41.223	−3.822	−45.045	−58.297	−0.604

[a] Glide score.
[b] Glide van der Waals energy.
[c] Glide Coulomb energy.
[d] Glide energy.
[e] Glide model energy.
[f] Hydrogen bond energy.

Table 5
Table showing docking results of selected ligands in the catalytic pocket of MurE enzyme (pdb.4C13).

Ligands	[a]G_{score}	[b]G_{vdw}	[c]G_{coul}	[d]G_{energy}	[e]G_{model}	[f]H_{Bond}
Ciglitazone	−3.581	−23.11	−7.498	−30.608	−39.12	−1.376
Pioglitazone	−4.129	−26.812	−7.654	−34.465	−46.423	−1.71
Englitazone	−4.157	−32.008	−1.997	−34.006	−43.606	−0.70
Darglitazone	−4.529	−33.213	−17.082	−50.296	−62.069	−1.059
Rosiglitazone	−3.655	−32.112	−17.831	−49.944	−54.338	−0.711
Netoglitazone	−3.171	−31.359	−11.153	−42.512	−53.772	−0.45
Rivoglitazone	−4.884	−30.061	−10.557	−40.618	−53.329	−2.189

[a] Glide score.
[b] Glide van der Waals energy.
[c] Glide Coulomb energy.
[d] Glide energy.
[e] Glide free model energy.
[f] Hydrogen bond energy.

Rivoglitazone also showed high negative values of binding free energies in the catalytic pockets of both enzymes ParE (87.76 kcal/mol, Table 6) and MurE (64.58 kcal/mol, Table 7) in contrast to other glitazones. Whereas the known inhibitor novobiocin has the highest glide score in the catalytic pocket of 4C13 (−7.985 kcal/mol) whereas it exhibited lower glide score (−5.174 kcal/mol, Table 3) than rivoglitazone in the catalytic pocket of 4MOT. The binding free energy results computed by Prime MM-GBSA are provided for both 4MOT and 4C13 enzymes in Tables 6 and 7, respectively.

Interactions of ligands with ParE

The docking result of novobiocin exhibited four hydrogen bonding interactions with the catalytic pocket of ParE involving Thr172, Asp78, Met87 andArg140 (Fig. 2a). While rivoglitazone formed three hydrogen bonds one each with Asn51, Ser124, and Arg140 (Fig. 2h). This compound contains a central phenyl ring which established a π-cationic interaction with the protonated NH_2 of Arg81. The other selected ligands showed similar interactions but to a lesser extent. In general, a hydrogen bonding interaction with Lys112 residue was exhibited by ciglitazone, pioglitazone, englitazone, rosiglitazone, and netoglitazone. However, a π–π interaction was observed between the electron cloud of the oxazole nucleus of darglitazone and phenyl ring of Tyr111 (Fig. 2e). Netoglitazone also established a π-cationic interaction with the protonated NH_2 of Arg79 (Fig. 2g).

Interactions of ligands with MurE

Most of the selected ligands occupied all three domains of the catalytic pocket (pdb.4C13) and formed hydrogen bonding interactions with Asn151 and Thr152. The extra-precision docked pose of novobiocin revealed six hydrogen bonding interactions mainly in the C-terminal region and central domain of MurE, involving the residues Ala150, Asp151, Thr152, His205, Tyr462 and His468 (Fig. 3a). Whereas rivoglitazone forms three hydrogen bonding interactions with

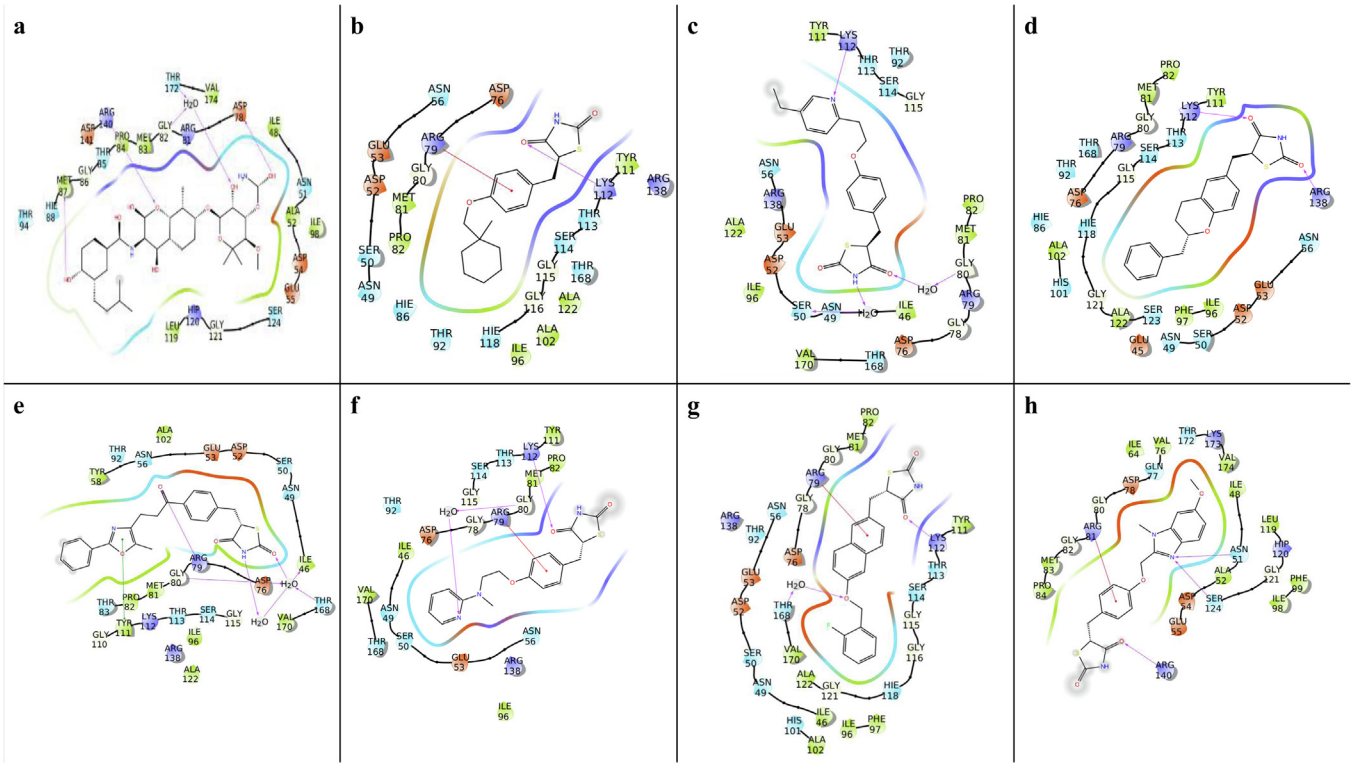

Fig. 2. Represents binding poses of (a) Novobiocin (b) Ciglitazone (c) Pioglitazone (d) Englitazone (e) Darglitazone (f) Rosiglitazone (g) Netoglitazone (h) Rivoglitazone within the catalytic pocket of ParE (pdb.4MOT).

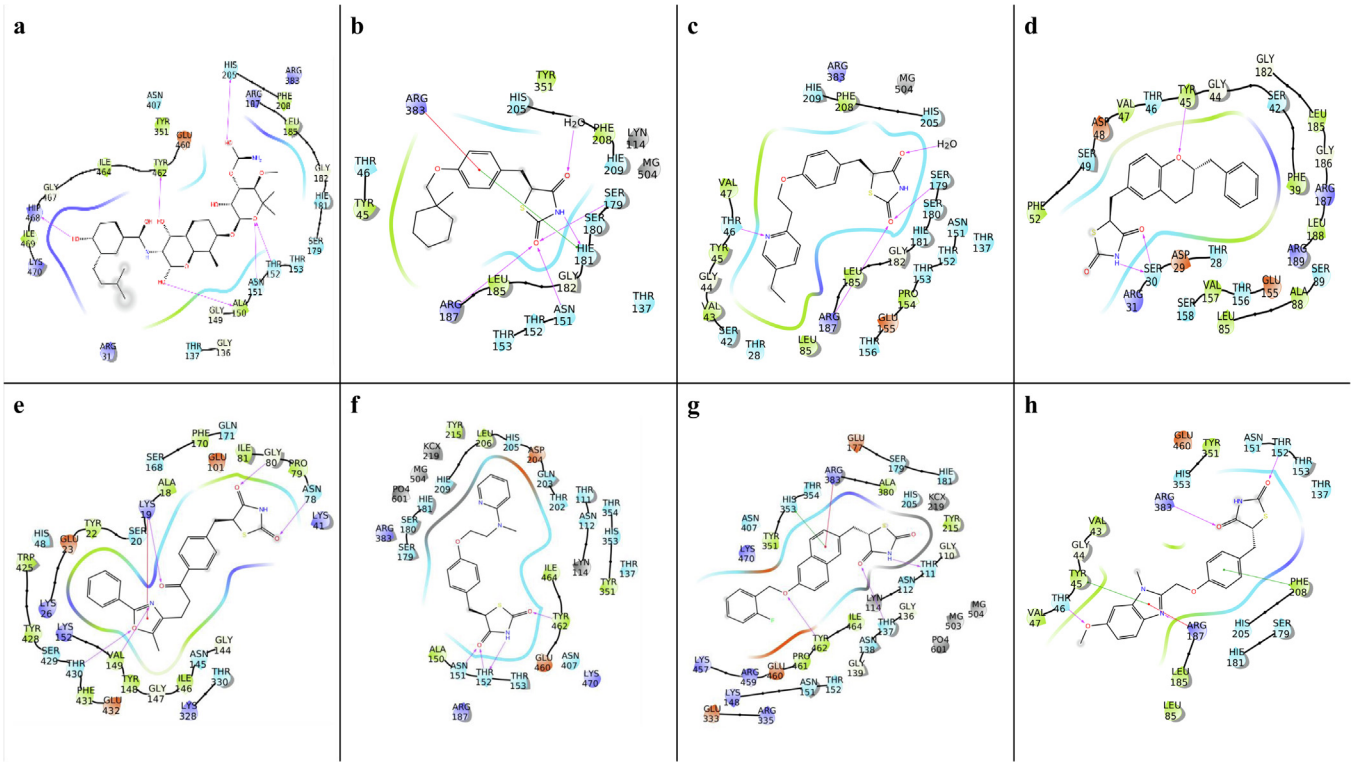

Fig. 3. Represents binding poses of (a) Novobiocin (b) Ciglitazone (c) Pioglitazone (d) Englitazone (e) Darglitazone (f) Rosiglitazone (g) Netoglitazone (h) Rivoglitazone with in the pocket of MurE (pdb.4C13).

Table 6
Table showing binding free energy (kcal/mol) of selected ligands in the catalytic pocket of ParE (pdb.4MOT) enzyme computed by the MM-GBSA approach.

Ligand	[a]ΔG_{bind}	[b]ΔG_{coul}	[c]ΔG_{cov}	[d]ΔG_{Hbond}	[e]ΔG_{lipo}	[f]ΔG_{solvGB}	[g]ΔG_{vdw}
Ciglitazone	−51.51	−20.74	8.88	−3.52	−19.18	29.22	−43.15
Pioglitazone	−63.74	−2.86	6.56	−1.9	−22.28	16.51	−56.43
Englitazone	−70.73	−3.21	−5.29	−3.12	−23.1	29.67	−58.16
Darglitazone	−61.33	−30.57	2.46	−4.28	−18.32	55.81	−61.86
Rosiglitazone	−58.65	−25.68	6.58	−4.73	−22.12	53.87	−61.02
Netoglitazone	−77.89	−11.14	6.55	−2.62	−27.53	36.03	−70.22
Rivoglitazone	−87.76	−27.53	8.17	−2.04	−26.8	46.18	−76.14

[a] Free energy of binding.
[b] Coulomb energy.
[c] Covalent energy (internal energy).
[d] Hydrogen bonding energy.
[e] Hydrophobic energy (nonpolar contribution estimated by solvent accessible surface area).
[f] Electrostatic solvation energy.
[g] van der Waals energy.

Table 7
Table showing binding free energy (kcal/mol) of selected ligands in the catalytic pocket of MurE (pdb.4C13) enzyme computed by the MM-GBSA approach.

Ligand	[a]ΔG_{bind}	[b]ΔG_{coul}	[c]ΔG_{cov}	[d]ΔG_{Hbond}	[e]ΔG_{lipo}	[f]ΔG_{solvGB}	[g]ΔG_{vdw}
Ciglitazone	−29.97	12.53	−7.60	−1.83	−9.12	14.16	−33.20
Pioglitazone	−52.59	26.14	5.80	−2.08	−20.6	−5.82	−49.09
Englitazone	−63.04	−69.49	10.3	−2.49	−24.11	63.44	−39.14
Darglitazone	−29.37	−25.1	−5.08	−3.03	−7.90	52.76	−33.61
Rosiglitazone	−69.92	−97.08	8.05	−5.42	−13.31	82.53	−41.29
Netoglitazone	−65.26	−101.89	25.4	−3.67	−20.66	86.00	−46.35
Rivoglitazone	−64.58	−33.37	3.28	−4.55	−10.42	21.37	−32.81

[a] Free energy of binding.
[b] Coulomb energy.
[c] Covalent energy (internal energy).
[d] Hydrogen bonding energy.
[e] Hydrophobic energy (nonpolar contribution estimated by solvent accessible surface area).
[f] Electrostatic solvation energy.
[g] van der Waals energy.

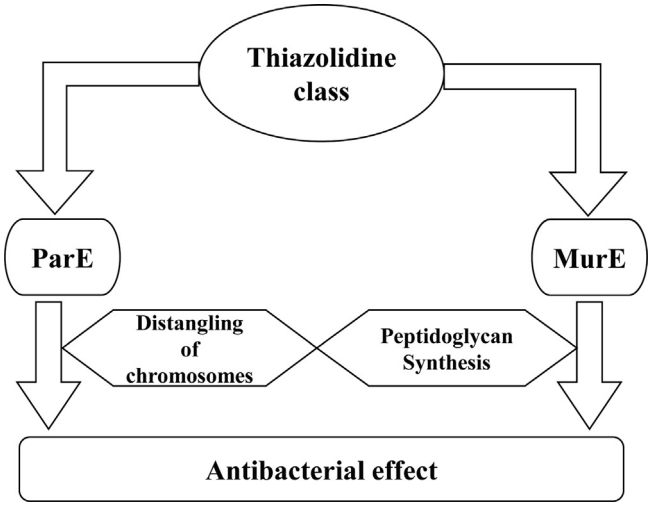

Fig. 4. Schematic representation of the mechanism of antibacterial activity by thiazolidine class of drugs targeting ParE and MurE enzymes.

Thr46, Thr152 and Arg383 residues present in the N-terminal and C-terminal domain of active site (Fig. 3h). This ligand further stabilized by π- π interaction of benzimidazole moiety of rivoglitazone with the phenyl ring of Tyr45. A π-cationic interaction was also observed between the benzimidazole moiety of rivoglitazone and the protonated NH_2 group of Arg187 (Fig. 3h).

Ciglitazone showed four hydrogen bonding interactions one each with His181, Asn151, Ser179, Arg187 key residues (Fig. 3b). This ligand was further stabilized by π- π interaction of phenyl ring with the imidazole ring of His181. A π-cationic interaction was also observed between the phenyl ring of ciglitazone and the protonated NH_2 group of Arg383 (Fig. 3b). On the other side darglitazone established four hydrogen bonding interactions one each with Lys19, Asn78, Gly80, Val149, Thr430 residues (Fig. 3e). In the case of englitazone, only two hydrogen bonding interactions were observed with Tyr45 and Ser30 residues (Fig. 3d). Whereas three hydrogen bonding interactions were observed for rosiglitazone, one each with Asp151, Thr152, and Tyr462 residues. Netoglitazone established three hydrogen bonding interactions, one each with Thr111, Thr137, Tyr462 key binding residues (Fig. 3g). Netoglitazone contains a central naphthyl ring which established a π-cationic interaction with the protonated NH_2 of Arg383. Further, this ligand is stabilized by one π-π interaction, observed between naphthyl group of netoglitazone and imidazole ring of His353.

Binding free energy calculations

In the present study, the binding free energy of all the ligands was computed by MM-GBSA [32] approach to get a better estimate of the binding strengths and relative potencies against MurE and ParE. It is evident from the energy components of the calculated binding free energies hat the major favorable contributors in case of 4MOT to the ligand binding are van der Waals (ΔG_{vdW}) and electrostatic solvation energy terms (ΔG_{solvGB}). The ΔG_{vdW} against ParE lies between −43.15 to −76.14 kcal/mol whereas in most of the selected ligands ΔG_{solvGB} disfavors binding −16.51 and 55.81 kcal/mol. And for 4C13 ΔG_{vdW}, coulomb energy (ΔG_{cou}) and ΔG_{solvGB} terms were found to be favorable contributors. The van der Waals interaction, coulombic energy and solvation energy in docked complexes against 4C13 ranges between −32.81 and −49.09 kcal/mol, −12.53 and 101.89 kcal/mol, −5.82 and 86.00 respectively in case of 4C13.

Nevertheless, rivoglitazone exhibited highest binding affinity with 4MOT (ΔG −87.76 kcal/mol) and also showed a higher contribution from van der Waals (−76.14 kcal/mol) However, the rivoglitazone exhibited lower binding affinity against 4C13 (ΔG −64.58 kcal/mol) as compared to other ligands in the study. Hence, it is clearly evident that binding free energies for all the ligands were contributed by van der Waals and electrostatic solvation energies against ParE and MurE enzymes. In addition, coulombs energy term is also found to be a favorable contributor for MurE.

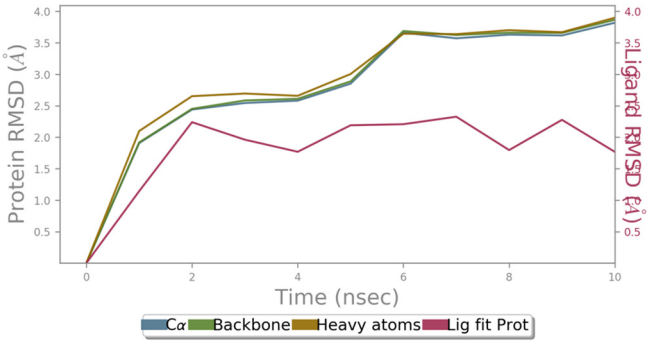

Fig. 5a. Represents the root mean square deviations (RMSDs) (Å) of the simulated positions of rivoglitazone/4MOTcomplex backbone atoms from those in the initial structure.

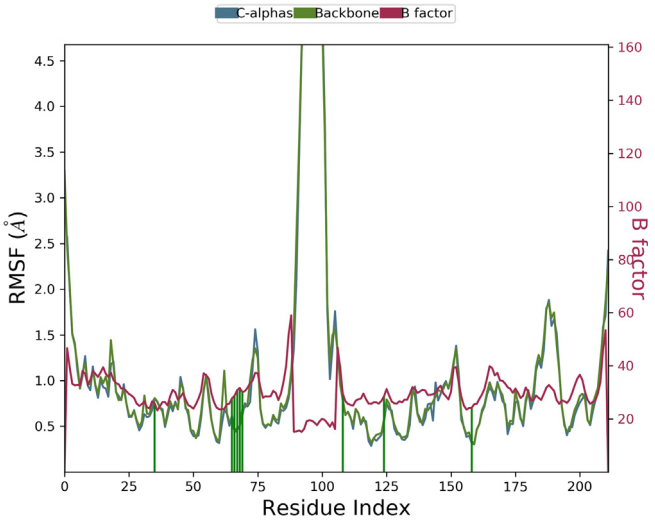

Fig. 5b. Represents the protein root mean square fluctuations (RMSF) (Å) of the simulated positions of rivoglitazone/4MOT complex backbone atoms from those in the initial structure.

Molecular dynamic (MD) simulations

In order to validate the docking results and stabilities of rivoglitazone/4MOT and rivoglitazone/4C13 complexes, 10 ns molecular dynamics (MD) simulations were carried out using Desmond [39] with an OPLS3 force field. Dynamics simulations were performed with explicit TIP4P water [40,41] in an orthorhombic box using the protocols as described earlier [42]. MD trajectory analysis of rivoglitazone/4MOT complexes exhibited hydrogen bonding, π-cationic and hydrophobic interactions which were observed from (Figs. 5c and d). MD trajectory of the rivoglitazone/4C13 complex also exhibited hydrogen bonding, π-cationic and hydrophobic interactions in the catalytic pocket of 4C13 (Figs. 6c and d).

Discussion

Although a myriad of research articles is available, our understanding of bacterial infections is still limited. However, of the various processes and mechanisms involved, ParE and MurE mediated bacterial infection is reported [41,42]. The rationale behind the selection of these

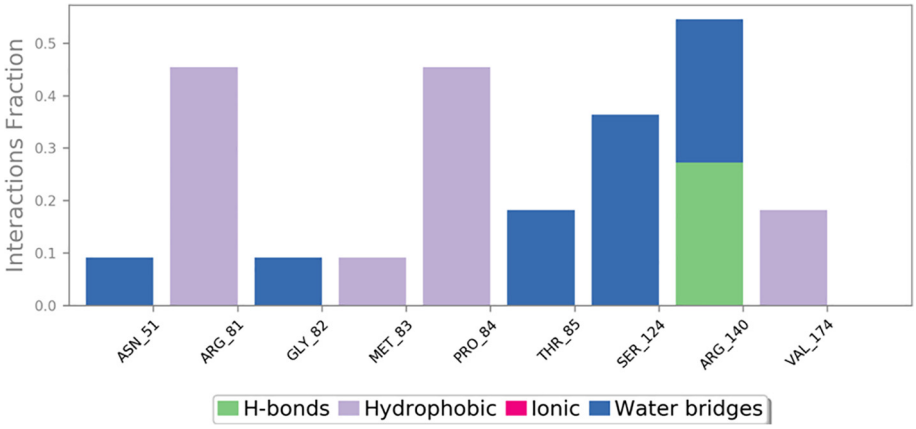

Fig. 5c. Plot represents the interaction of rivoglitazone with different residues of enzyme 4MOTthroughout the molecular dynamics (MD) simulation trajectory.

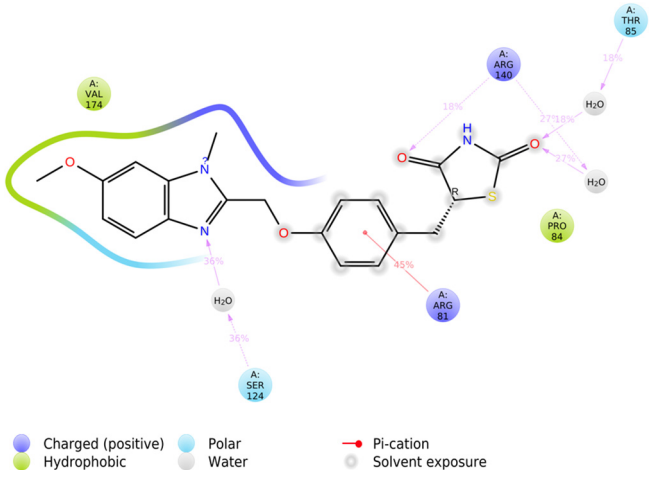

Fig. 5d. Represents the interaction of rivoglitazone with catalytic pocket residues of 4MOT during MD simulation.

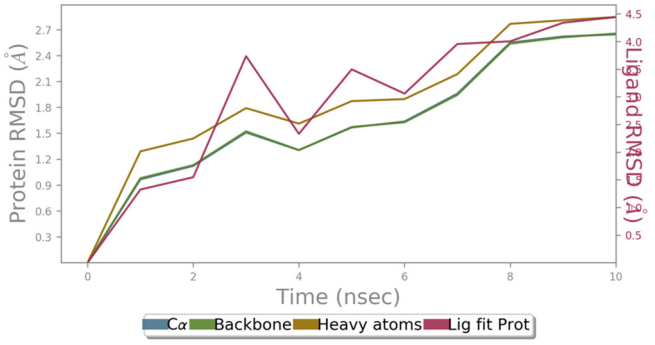

Fig. 6a. Represents the RMSDs (Å) of the simulated positions of rivoglitazone/4C13 complex backbone atoms from those in the initial structure.

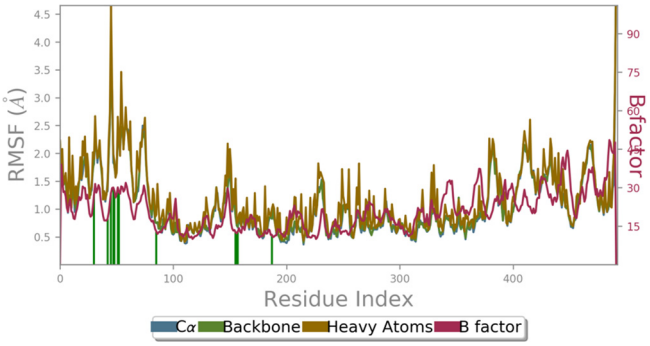

Fig. 6b. Represents the protein root mean square fluctuations (RMSF) (Å) of the simulated positions of rivoglitazone/4C13 complex backbone atoms from those in the initial structure.

two receptors is mainly the function of receptors in bacteria. The ParE enzyme is considered to be an important target for antibacterial agents. As this is less prone to resistance when compared to GyrB which belongs to the same class of topoisomerases [43]. On the other hand, MurE involved in the bacterial peptidoglycan synthesis and these two receptors are unexploited in nature. The approach of targeting unexploited targets results in the resistance-free environment [44].

Thiazolidine class of drugs, for example, pioglitazone, an antidiabetic drug frequently investigated for antibacterial effect [24]. So, the compounds containing thiazolidine moiety in its chemical structure have also been tested for the antibacterial property. The current study reveals that rivoglitazone is considered as a potent antibacterial drug, as it shows higher glide scores when compared to other thiazolidine class of drugs and also novobiocin, a potent antibacterial drug selected as a standard for comparison. In the case of novobiocin, interactions are mainly observed in the central and C-terminal domains of MurE catalytic pocket. Whereas in the case of rivoglitazone interactions are observed in the N-terminal and central domains. In the case of the ParE enzyme, the benzimidazole moiety of rivoglitazone is located in the region of catalytic pocket surrounded by charged residues. Whereas in the case of novobiocin most part of the molecule is surrounded by the hydrophobic residues.

The higher negative g-score of rivoglitazone is mainly because of the availability of effective functional groups in the chemical structure of rivoglitazone. The 6-methoxy-1-methyl-1*H*-benzo[*d*]imidazole moiety at the para position of the phenoxy group contributes to the maximum interactions with the catalytic domain of both antibacterial receptors. The extra-precision docked pose of rivoglitazone against ParE (pdb.4MOT) revealed three hydrogen bonding interactions one each with Asn51, Ser124, and Arg140. This ligand contains a central phenyl ring which established a π-cationic interaction with the protonated NH_2 of Arg81. The extra-precision docked pose of rivoglitazone against MurE (pdb.4C13) revealed three hydrogen bonding interactions with Thr46, Thr152 and Arg383 residues present in the N-terminal and C-terminal domain of the active site. This ligand further stabilized by two π- π interaction, one with benzimidazole moiety of rivoglitazone and phenyl ring of Tyr45 and the other with central phenyl ring of rivoglitazone and phenyl ring of Phe208. A π-cationic interaction was also observed between the benzimidazole moiety of rivoglitazone and the protonated NH_2 group of Arg187.

The higher free binding energy of rivoglitazone reveals the binding affinity against the two receptors which play a crucial role as

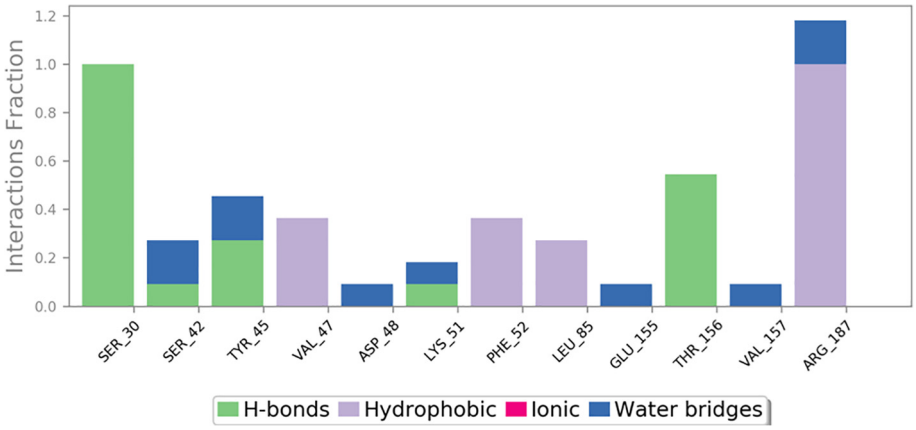

Fig. 6c. Plots represents the interaction of rivoglitazone with different residues of enzyme 4C13throughout the molecular dynamics (MD) simulation trajectory.

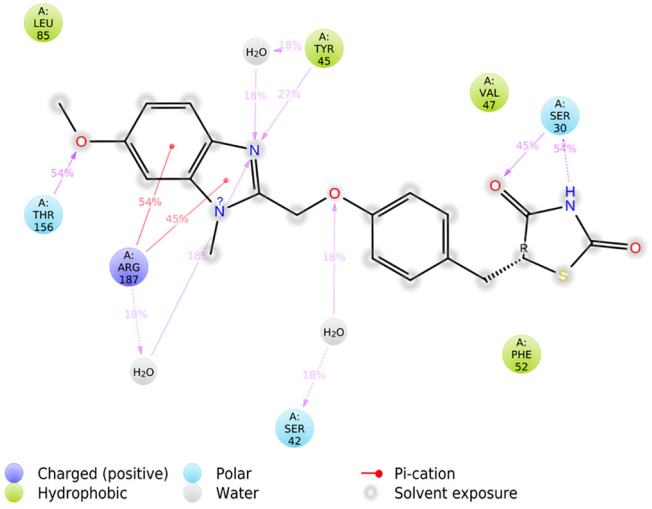

Fig. 6d. Represents the interaction of rivoglitazone with catalytic pocket residues of 4C13 during MD simulation.

antibacterial targets. In extra-precision docking rivoglitazone showed highest glide score for both target proteins 4MOT (−5.204 kcal/mol), 4C13 (−4.884 kcal/mol) compared to the other glitazones. It is evident that rivoglitazone has a higher affinity for the ParE (−5.204 kcal/mol, Table 4) than novobiocin (−5.174 kcal/mol, Table 4) and has lower affinity for the MurE in comparison to novobiocin (−7.985 kcal/mol). The free energy calculations of a protein ParE with novobiocin elicits binding free energy (ΔG_{bind}) of −51.912 kcal/mol, which is less as compared to the ΔG_{bind} of rivoglitazone (−87.76 kcal/mol). It is also evident from Table 7 that rivoglitazone has higher ΔGbind in comparison with other glitazones (Tables 6 and 7) in the study. Novobiocin exhibited a higher negative value of ΔG_{bind} of −88.52 kcal/mol with MurE compared to the ΔG_{bind} of rivoglitazone −64.58 kcal/mol. Although the drug rosiglitazone showed higher ΔG_{bind} score −69.92 kcal/mol with respect to rivoglitazone, the highest docking score is availed by the rivoglitazone among all other glitazones preferred in the study. Thus, findings obtained in the current study indicate that rivoglitazone scaffold can be a better choice for the development of novel antibacterial agents (Fig. 4).

During MD simulation of rivoglitazone/4MOT complex, RMSD values of protein all backbone and C-α atoms were calculated relative to the start of the 10 ns MD run (Fig. 5a). The complex backbone and C-α atom RMSDs increased to 3.56 and 3.52 Å, respectively, during equilibration and then became stable in the range 3.54–3.57 Å and 3.52–3.54 Å during the rest of the simulation time. This indicated no significant structural changes in protein structure. Fig. 5a also indicates that RMSD of catalytic pocket residues copes well with the ligand movement. RMSF values of catalytic pocket binding residues were observed in the range 0.42–0.75 Å (Fig. 5b), further indicating the fewer fluctuations of catalytic pocket residues. MD trajectory analysis of rivoglitazone/4MOT complex showed hydrogen bonding, π-cation and hydrophobic interactions (Figs. 5c and d). Precisely, the central phenyl ring exhibited π-cationic interaction with protonated NH_2 of Arg81 for 45% of the MD trajectory. A medium frequency hydrogen bonding interaction was observed between the nitrogen atom of the N-methyl benzimidazole ring and Ser124 (36% of the MD trajectory). Another medium frequency water-mediated hydrogen bonding interaction (27% of the MD trajectory) was observed between one of the carbonyl oxygen of thiazolidine-2,4-dione ring and Arg140. This carbonyl oxygen also showed low-frequency hydrogen bonding interaction with Thr85 (27% of the MD trajectory). It is also evident from the interaction fraction diagram (Fig. 5c) that this ligand is further stabilized within the catalytic pocket by hydrophobic interaction with Pro84. Above results indicate that apart from hydrogen bonding, hydrophobic and ionic interactions are crucial for the stabilization of inhibitor within the catalytic pocket.

During MD simulation of rivoglitazone/4C13 complex, all backbone, and C-α atoms RMSD sharply increased up to 2.44 and 2.43 Å, respectively during the equilibration phase. Then it was stabilized in the range of 2.43–2.52 Å (backbone atoms) and 2.42–2.50 Å (C-α atoms) (Fig. 6a). This indicated the stability of the complex during the rest of the simulation time. RMSF of catalytic pocket binding residues was observed in the range 0.52–1.41 Å (Fig. 6b), further indicating fewer fluctuations in catalytic pocket residues and stability of the complex. Like 4MOT, rivoglitazone also exhibited hydrogen bonding, π-cationic and hydrophobic interactions in the catalytic pocket of 4C13 (Figs. 6c and d). Protonated NH_2 of Arg187 exhibited two high-frequency π-cationic interactions, one each with imidazole (45% of the MD trajectory) and benzo part (54% of the MD trajectory) of the N-methyl benzimidazole ring. A high-frequency hydrogen bonding interaction (54% of the MD trajectory) was observed between the oxygen of methoxy moiety present on the N-methyl benzimidazole ring with Thr156. Ser30 of N-terminal domain exhibited two high-frequency hydrogen bonding interactions, one each with NH (54% of the MD trajectory) and one of the carbonyl oxygen (45% of the MD trajectory) of thiazolidine-2,4-dione ring. A medium frequency hydrogen bonding interaction (27% of the MD trajectory) was also observed between nitrogen atom present on the third position of the N-methyl benzimidazole ring and Tyr45. Rivoglitazone also exhibited three low-frequency hydrogen bonding interaction (18% of the MD trajectory in each case) with Ser42, Tyr45, and Arg 187 residues. These results are in agreement with our extra-precision docking result (Figs. 2 and 3).

Conclusion

The hypothesized current study demonstrates that rivoglitazone, an oral hypoglycaemic agent belonging to the thiazolidine-2,4-dione class of drug has potentially interacted with the binding pocket residues of ParE (pdb.4MOT) and MurE (pdb.4C13), validated targets for antibacterial agents. Molecular docking and binding free energy calculations were employed as a computational tool to validate this hypothetical study. Further, MD simulation studies were performed to validate the docking result and stability of rivoglitazone/4MOT and rivoglitazone/4C13 complexes. MD simulation studies showed that apart from hydrogen bonding interaction, π-cationic and hydrophobic interactions also play a crucial role in the stabilization of inhibitor with the catalytic pockets. The thiazolidine class of drugs has the potential to inhibit the target ParE and MurE enzymes. Thus, it is speculated that the inhibitory effect of rivoglitazone on ParE and MurE enzymes may inhibit the peptidoglycan biosynthetic pathway with ultimate bacterial cell death. Rivoglitazone scaffold may be used for the development of effective antibacterial agent for the treatment of bacterial infections. This requires further investigations regarding *in vitro* and *in vivo* studies.

Author's contribution

Yele Vidyasrilekha was the author, synthesized the literature, involved in drafting the paper and critical revision of the manuscript. Niladri Saha involved in computational studies. Dr. Md. Afzal Azam provided conceptual inputs. All authors read and approved the final paper.

Acknowledgment

The authors greatly acknowledge the All India Council of Technical Education, National doctoral fellowship (NDF-2018), India, Application number: 56149, dated: 25.07.2018 for providing the fellowship support.

Declaration of Competing Interest

The authors declare that there are no conflicts of interest in this study. The authors alone are responsible for the content and writing of the paper.

Appendix A. Supplementary data

Supplementary data to this article can be found online at https://doi.org/10.1016/j.mehy.2019.109305.

References

[1] Li B, Webster TJ. Bacteria antibiotic resistance: new challenges and opportunities for implant-associated orthopedic infections. J Orthop Res 2018;36:22–32.
[2] Neu HC. The crisis in antibiotic resistance. Science 1992;257:1064–73.
[3] Carlet J, Jarlier V, Harbarth S, Voss A, Goossens H, Pittet D. Ready for a world without antibiotics? The pensières antibiotic resistance call to action. BioMed Central 2012;11.
[4] Blair JM, Webber MA, Baylay AJ, Ogbolu DO, Piddock LJ. Molecular mechanisms of antibiotic resistance. Nat Rev Microbiol 2015;13:42.
[5] Lambert PA. Bacterial resistance to antibiotics: modified target sites. Adv Drug Deliv Rev 2005;57:1471–85.
[6] Santajit S, Indrawattana N. Mechanisms of antimicrobial resistance in ESKAPE pathogens. BioMed Res Int 2016;2016.
[7] Poole K. Efflux pumps as antimicrobial resistance mechanisms. Ann Med 2007;39(3):162–76.
[8] Tsiodras S, Gold HS, Sakoulas G, Eliopoulos GM, Wennersten C, Venkataraman L, et al. Linezolid resistance in a clinical isolate of *Staphylococcus aureus*. Lancet 2001;358:207–8.
[9] Sabol K, Patterson JE, Lewis JS, Owens A, Cadena J, Jorgensen JH. Emergence of daptomycin resistance in Enterococcus faecium during daptomycin therapy. Antimicrob Agents Chemother 2005;49:1664–5.
[10] Saravolatz LD, Stein GE, Johnson LB. Ceftaroline: a novel cephalosporin with activity against methicillin-resistant *Staphylococcus aureus*. Clin Infect Dis 2011;52:1156–63.
[11] O'Neil J. The Review on antimicrobial resistance. Antimicrobial resistance: tackling a crisis for the health and wealth of nations UK, HM Government Report: AMR ORG; 2014:pp. 1–20.
[12] Green DW. The bacterial cell wall as a source of antibacterial targets. Expert Opin Ther Targets 2002;6:1–20.
[13] Tomacic T, Zidar N, Kovac A, Turk S, Simcic M, Blanot D, Muller-Premru M, Filipic M, Grdadolnik SG, Zega A, Anderluh M. 5-Benzylidenethiazolidin-4-ones as multi-target inhibitors of bacterial Mur ligases. Chem Med Chem 2010;5:286–95.
[14] Wright HT, Reynolds KA. Antibacterial targets in fatty acid biosynthesis. Curr Opin Microbiol 2007;10:447–53.
[15] Bai H, Zhou Y, Hou Z, Xue X, Meng J, Luo X. Targeting bacterial RNA polymerase: promises for future antisense antibiotics development. Infect Disord Drug Targets 2011;11:175–87.
[16] Bourne C. Utility of the biosynthetic folate pathway for targets in antimicrobial discovery. Antibiotics 2014;3:1–28.
[17] Estrada A, Wright DL, Anderson AC. Antibacterial antifolates: from development through resistance to the next generation. Cold Spring Harb Perspect Med 2016;6:a028324.
[18] Azam MA, Thathan J, Jubie S. Dual targeting DNA gyrase B (GyrB) and topoisomerse IV (ParE) inhibitors: a review. Bioorg Chem 2015;62:41–63.
[19] Arenz S, Wilson DN. Bacterial protein synthesis as a target for antibiotic inhibition. Cold Spring Harb Perspect Med 2016;6(9):a025361.
[20] Chopra I, Roberts M. Tetracycline antibiotics: mode of action, applications, molecular biology, and epidemiology of bacterial resistance. Microbiol Mol Biol Rev 2001;65:232–60.
[21] Kotra LP, Haddad J, Mobashery S. Aminoglycosides: perspectives on mechanisms of action and resistance and strategies to counter resistance. Antimicrob Agents Chemother 2000;44:3249–56.
[22] Mazzei T, Mini E, Novelli A, Periti P. Chemistry and mode of action of macrolides. J Antimicrob Chemoth 1993;31(suppl_C):1–9.
[23] Silver LL. Challenges of antibacterial discovery. Clin Microbiol Rev 2011;24:71–109.
[24] Masadeh MM, Mhaidat NM, Al-Azzam SI, Alzoubi KH. Investigation of the antibacterial activity of pioglitazone. Drug Des Devel Ther 2011;5:421.
[25] Tomasic T, Masic LP. Rhodanine as a privileged scaffold in drug discovery. Curr Med Chem 2009;16:1596–629.
[26] Rohatagi S, Carrothers TJ, Jin J, Jusko WJ, Khariton T, Walker J, et al. Model-based development of a PPARγ agonist, rivoglitazone, to aid dose selection and optimize clinical trial designs. J Clin Pharmacol 2008;48:1420–9.
[27] Drlica K. Mechanism of fluoroquinolone action. Curr Opin Microbiol 1999;2:504–8.
[28] El Zoeiby A, Sanschagrin F, Levesque RC. Structure and function of the Mur enzymes: development of novel inhibitors. Mol Microbiol 2003;47:1–12.
[29] Sastry GM, Adzhigirey M, Day T, Annabhimoju R, Sherman W. Protein and ligand preparation: parameters, protocols, and influence on virtual screening enrichments. J Comput Aided Mol Des 2013;27:221–34.
[30] Jacobson MP, Pincus DL, Rapp CS, Day TJ, Honig B, Shaw DE, et al. A hierarchical approach to all-atom protein loop prediction. Proteins: Struct Funct Bioinf 2004;55:351–67.
[31] Azam MA, Jupudi S. Extra precision docking, free energy calculation and molecular dynamics studies on glutamic acid derivatives as MurD inhibitors. Comput Biol Chem 2017;69:55–63.
[32] Harder E, Damm W, Maple J, Wu C, Reboul M, Xiang JY, et al. OPLS3: a force field providing broad coverage of drug-like small molecules and proteins. J Chem Theory Comput 2016;12:281–96.
[33] Li J, Abel R, Zhu K, Cao Y, Zhao S, Friesner RA. The VSGB 2.0 model: a next generation energy model for high resolution protein structure modeling. Proteins Struct Funct Bioinf 2011;79:2794–812.
[34] Guo Z, Mohanty U, Noehre J, Sawyer TK, Sherman W, Krilov G. Probing the α-helical structural stability of stapled p53 peptides: molecular dynamics simulations and analysis. Chem Biol Drug Des 2010;75:348–59.
[35] Jorgensen WL, Chandrasekhar J, Madura JD, Impey RW, Klein ML. Comparison of simple potential functions for simulating liquid water. J Chem Phys 1983;79:926–35.
[36] Lawrence C, Skinner J. Flexible TIP4P model for molecular dynamics simulation of liquid water. Chem Phys Lett 2003;372:842–7.
[37] Essmann U, Perera L, Berkowitz ML, Darden T, Lee H, Pedersen LG. A smooth particle mesh Ewald method. J Chem Phys 1995;103:8577–93.
[38] Hoover WG. Constant-pressure equations of motion. Phys Rev A 1986;34:2499.
[39] Martyna GJ, Klein ML, Tuckerman M. Nosé-Hoover chains: the canonical ensemble via continuous dynamics. J Chem Phys 1992;97:2635–43.
[40] Martyna GJ, Tobias DJ, Klein ML. Constant pressure molecular dynamics algorithms. J Chem Phys 1994;101:4177–89.
[41] Blondeau JM. Fluoroquinolones: mechanism of action, classification, and development of resistance. Sur Ophthalmol 2004;49:S73–8.
[42] Reynolds PE. Structure, biochemistry and mechanism of action of glycopeptide antibiotics. Eur J Clin Microbiol 1989;8:943–50.
[43] Eaves DJ, Randall L, Gray DT, Buckley A, Woodward MJ, White AP, et al. Prevalence of mutations within the quinolone resistance-determining region of gyrA, gyrB, parC, and parE and association with antibiotic resistance in quinolone-resistant Salmonella enterica. Antimicrob Agents Chemother 2004;48:4012–5.
[44] Worthington RJ, Melander C. Combination approaches to combat multidrug-resistant bacteria. Trends Biotechnol 2013;31:177–84.
[45] Kale RR, Kale MG, Waterson D, Raichurkar A, Hameed SP, Manjunatha M, et al. Thiazolopyridone ureas as DNA gyrase B inhibitors: optimization of antitubercular activity and efficacy. Bioorg Med Chem Lett 2014;24:870–9.
[46] Ruane KM, Lloyd AJ, Fülöp V, Dowson CG, Barreteau H, Boniface A, et al. Specificity determinants for lysine incorporation in *Staphylococcus aureus* peptidoglycan as revealed by the structure of a MurE enzyme ternary complex. J Biol Chem 2013;288:33439–48.